Passive Gust Loads Alleviation in a Truss-Braced Wing using an Inerter-Based Device

Christopher P. Szczyglowski*, Simon A. Neild†, Branislav Titurus‡ and Jason Z. Jiang§
Faculty of Engineering, University of Bristol, United Kingdom

Etienne Coetzee¶
Airbus, Filton, Bristol, BS34 7PA, United Kingdom

This paper presents a novel method for gust loads alleviation in a truss-braced wing in which an inerter-based device located in the truss-structure is used to reduce peak-loads during a discrete '1-cosine' gust. Three candidate layouts are considered and the device parameters are optimised to target the response of the first three structural modes. It is demonstrated that either a single damper or a combination of inerter-based devices can be used to achieve a reduction of approximately 4% for spanwise locations inboard of the strut attachment point and that this reduction is consistent across the full range of gust gradients. Furthermore, it is noted that the inerter-based device has a significantly smaller damping coefficient than the case where just a damper is used and that the device parameter values are viable within the scope of an aerospace application.

I. Introduction

In recent years a significant effort has been devoted to the study of more energy efficient aircraft that will meet the environmental performance goals set out in initiatives such as Vision 2020 and Flight Path 2050. Some of these studies have considered the implementation of new aircraft concepts that can provide enhanced performance in terms of overall aircraft efficiency and noise [1].

One such concept is the truss-braced wing (TBW) aircraft which uses a bracing structure underneath the wing to achieve a higher aspect ratio design. The addition of the truss leads to a structurally efficient design with reduced weight and lower induced drag from the increased aspect ratio, however, the truss structure generates interference drag that must be traded as part of a comprehensive multidisciplinary optimisation study [2–4]. Despite this, it has been shown that the TBW concept can provide improvements in maximum take-off weight and fuel burn over a traditional cantilevered-wing design if the interface between the truss structure and the wing is properly designed. Recently, Malik *et al.* [5] identified

*Postgraduate Student, Department of Aerospace Engineering, Queen's Building, University Walk, Bristol, BS8 1TR.
†Professor of Nonlinear Structural Dynamics, Department of Mechanical Engineering.
‡Senior Lecturer in Aerospace Dynamics, Department of Aerospace Engineering
§Senior Lecturer in Dynamics and Control, Department of Mechanical Engineering
¶Future Projects Engineer, Future Projects Office, Airbus Operations Ltd. Pegasus House, Aerospace Avenue, Filton, Bristol, BS34 7PA

that aeroelastic phenomena such as flutter are the main constraints which drive the overall design of the TBW aircraft, thereby placing a limit on the practical efficiency savings that can be achieved when considering a braced wing design. Furthermore, initial sizing studies conducted as part of the NASA and Boeing Subsonic Ultra Green Aircraft Research (SUGAR) project [6] have shown that gust loads are responsible for sizing many of the structural components in the wing box [7]. Hence, a primary requirement for the success of the TBW concept is to reduce the effect of these aeroelastic phenomena, thus enabling further reductions in wing weight which leads to a more efficient design.

A typical strategy to reduce gust loads is to enable loads control via aerodynamic control surfaces [8]. This approach is commonplace across the aerospace industry and has been applied to the SUGAR TBW aircraft during aeroelastic wind tunnel tests where it was observed to suppress flutter and alleviate gust loads, although the controller was not expressly designed for gust load alleviation (GLA)[9]. Recently, Bartels *et al.* [10] performed a study of GLA and flutter suppression in a TBW aircraft using the the Variable Camber Continuous Trailing Edge Flap (VCCTEF) concept coupled with a static output feedback controller. It was found that the controller was effective in suppressing flutter and stabilizing the aircraft during a gust encounter, however only a single gust gradient was considered during the controller design and the overall level of loads reduction is not quantified. Whilst active control schemes have been shown to suppress flutter and provide GLA, the certification of these systems and their integration into the design process does present a number of challenges [11], hence why other methods of loads alleviation been proposed such as folding wing tips [12], aeroelastic tailoring [13] and morphing structures [14]. In this paper an alternative approach to loads alleviation in a truss-braced wing is presented, which is to use a two-terminal vibration absorber embedded within the truss structure to reduce the gust response. Such an approach is not feasible in a cantilever wing as a location does not exist where the relative motion of the wing structure can be exploited by a two terminal device, however the addition of the truss-structure means there are now several candidate locations where a device could be placed. For example, if a hinge connection between the strut and the wing is employed then the rotation of the strut about that joint could be utilised or the jury-strut may experience significant relative motion due to the combined bending of the wing and the primary strut.

Vibration absorbers are common in many structures which undergo large motions or are subject to vibrations which are detrimental to the overall performance or health of the structure. Considering aerospace applications, for decades they have been used to ensure lead-lag stability of helicopter rotor blades [15] as well as alleviate landing loads and suppress shimmy in aircraft landing gear [16]. Typically these absorbers are restricted to a combination of springs, dampers and lumped masses [17], however, in 2002 Smith [18] introduced a mechanical element known as an inerter that is now being used extensively in the field of mechanical networks*. In recent years inerter-based devices have been identified for a wide-range of applications including the automotive [19], locomotive [20, 21] and civil engineering

*In this context a mechanical network is defined as a collection of spring, damper and inerter elements that are connected in series or parallel in a similar fashion to an electrical circuit diagram.

industries [22, 23]. Furthermore, inerter-based devices have been proposed to suppress shimmy [24] and improve touch down performance [25] in aircraft landing gear. These devices are particularly useful in aerospace applications as the inertance b can be much larger than the actual mass of the device via the use of gearing mechanisms [18].

Research into exploiting such devices on braced wings is limited. A telescopic strut design was proposed by Haftka *et al.* [26, 27] as part of an early MDO study at Virginia Tech, however the design of this device only considered a spring that had zero-stiffness in compression and no additional mechanical elements were included. Here we consider whether a single passive vibration absorber device, or a combination of devices, can be used to positively influence the gust response of a truss-braced wing. The *structure-based* approach to mechanical network design [28] is utilised and we consider both dampers and devices that have an internal degree-of-freedom (DOF) which allows the device to be frequency tuned to target specific modes of the structure.

The rest of the paper is organised as follows: In Section II the SUGAR-inspired truss-braced wing aeroelastic model is introduced and the method for optimising a vibration absorber to alleviate gust loads is discussed. In Section III the baseline gust response of the truss-braced wing model is presented, with specific emphasis on the gust loads envelope and the structural modes which are most active throughout the gusts. In Section IV and V the three candidate vibration suppression devices are included in the model and their effects on the gust loads envelope are observed for a range of parameter values. Finally, the main findings of the study are discussed and conclusions are presented along with suggestions for further work.

II. Modelling and Optimisation

This section is split into two parts: first, the SUGAR-inspired truss-braced wing aeroelastic model considered in this paper is introduced and the modelling methods used throughout the device optimisation process are discussed, then the framework for optimising a vibration absorber to alleviate gust loads is introduced and each module is described in turn.

A. Aeroelastic Model and Vibration Absorber Integration

Figure 1 shows the half-wing aeroelastic finite element model (FEM) that has been generated based on the 765-09 Rev. D version of the SUGAR Volt concept aircraft [7]. An overview of the FEM is provided in Table 1 and the main planform parameters are summarised in Tables 2 and 3. The FEM is a typical 'stick' model comprising of flexible beams for the wing, strut and jury-strut members and lumped masses are used to represent the mass and inertia of the structure. Figure 2 shows the beam stiffness values which have been derived from the full-scale FEM data provided in [7]. Note that the data in this report does not provide the axial stiffness - here it is taken to be one order of magnitude greater than the in-plane stiffness which is consistent with the modelling assumptions made by Su [29]. Data for the wing mass is derived from the full-fuel mass distribution given in Table 3.2 of [7] and the mass and rotational inertia distribution of the truss structure are taken from Su's paper on strut-braced wing modelling [29]. The engine is included

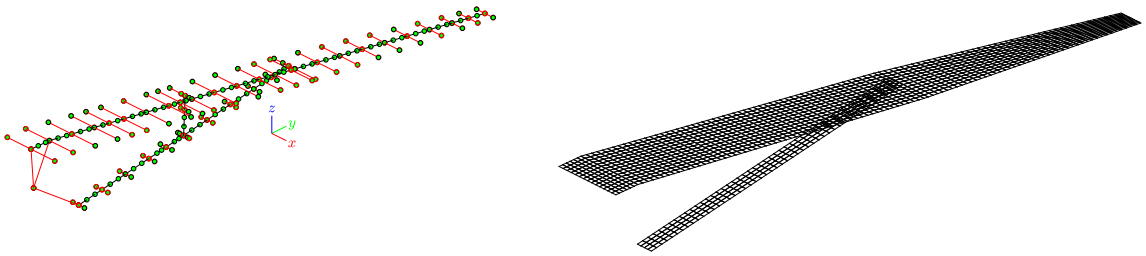

(a) Structural Model: Green - Nodes, Black - Flexible Beams, Red - Rigid Elements

(b) Aerodynamic Model

Fig. 1 Aeroelastic model of the truss-braced wing

Table 1 Mesh properties for the SUGAR-inspired half-wing FEM

Property	Value	Units
No. Structural DOF	1093	[-]
No. Aerodynamic DOF	1561	[-]
Beam Element Length	0.5	[m]
Aerodynamic Panel Length	0.2	[m]
Aerodynamic Panel Aspect Ratio	1	[-]

as a lumped mass of 3633kg which is derived from the data for the gFan+ in Table 2.35 of [7].

The beam axis is positioned at the midchord for all flexible members and rigid bars are connected to the beam nodes to represent the planform shape and provide the basis for the spline between the structural and aerodynamic DOFs. The connection between the truss members and the wing are modelled as pinned-joints which transfer both in-plane and torque moments across the joint, furthermore, the strut joins the wing at the front-spar location which provides passive loads alleviation to the wing bending moments and torques [30]. The wing and strut are joined to a reference node which is fully-fixed for all subsequent analysis, meaning that the rigid body modes will not participate in the gust response. This will have a significant effect on the participation of the flexible modes, however, as this is a preliminary investigation this simple approach is deemed satisfactory.

The commercial finite element analysis (FEA) software MSC Nastran™ is used throughout this study to conduct all

Table 2 Wing planform properties for the SUGAR-inspired aeroelastic model

	Wing Root	Wing-Fuselage Joint	Midboard Kink	Wing Tip
Spanwise Position [m]	0	1.27	14.93	25.90
Leading Edge Sweep [°]	0	11.88	16.74	16.74
Dihedral [°]	-1.5	-1.5	-1.5	-1.5
Chord [m]	3.28	3.28	2.91	1.15

Table 3 Strut and jury-strut planform properties for the SUGAR-inspired aeroelastic model

	Property	Value	Units
Strut	Root Coordinates (x,y,z)	(0, 3.29, -2.39)	[m]
	Tip Coordinates (x,y,z)	(2.65, 12.79, 0.9)	[m]
	Chord	0.8	[m]
Jury-Strut	Root Coordinates (x,y,z)	(1.33, 9.22, -0.33)	[m]
	Tip Coordinates (x,y,z)	(1.33, 9.22, 0.17)	[m]
	Chord	0.8	[m]

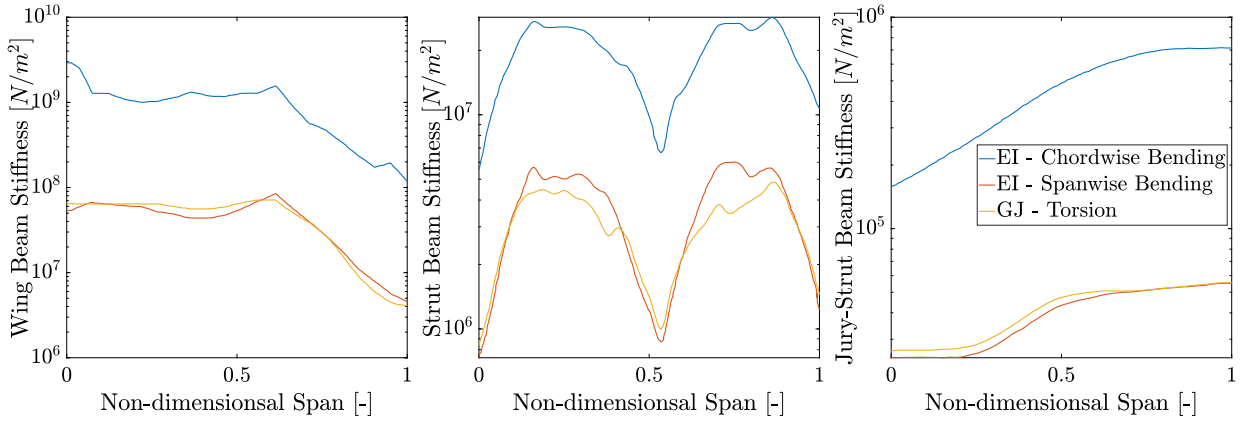

(a) Wing stiffness distribution **(b) Strut stiffness distribution** **(c) Jury-Strut stiffness distribution**

Fig. 2 Stiffness distribution for the (a) wing, (b) strut and (c) jury-strut

analysis and optimise the device parameters. The technique of modelling a generic vibration suppression device using a commercial FEA tool such as MSC Nastran has not been exploited by the mechanical network community, despite the required elements being readily available within these tools. In effect, the finite element approach provides a convenient way of modelling a vibration absorber attached to a host structure as one can construct any generic mechanical network by connecting spring, damper and/or inerter elements in series or parallel. In effect, the device can be thought of as a sub-structure within the larger model assembly with, for the case where one device is used, the existing structural mass, damping and stiffness matrices, M_s, C_s and K_s respectively, augmented as [31]

$$M = \begin{bmatrix} M_s + m_d w w^T & -m_d w \\ -m_d w^T & m_d \end{bmatrix}, C = \begin{bmatrix} C_s + c_d w w^T & -c_d w \\ -c_d w^T & c_d \end{bmatrix}, K = \begin{bmatrix} K_s + k_d w w^T & -k_d w \\ -k_d w^T & k_d \end{bmatrix} \tag{1}$$

where subscript s and d denote the terms belonging to the structure and the device respectively and the term w is a column vector of zeros and ones describing the connectivity between the device and the host structure. Note that multiple devices can be catered for by using Equation 1 iteratively. For the case where the elements are connected in series, new DOFs are introduced to the system via internal device-DOFs. In this instance the displacement-vector is

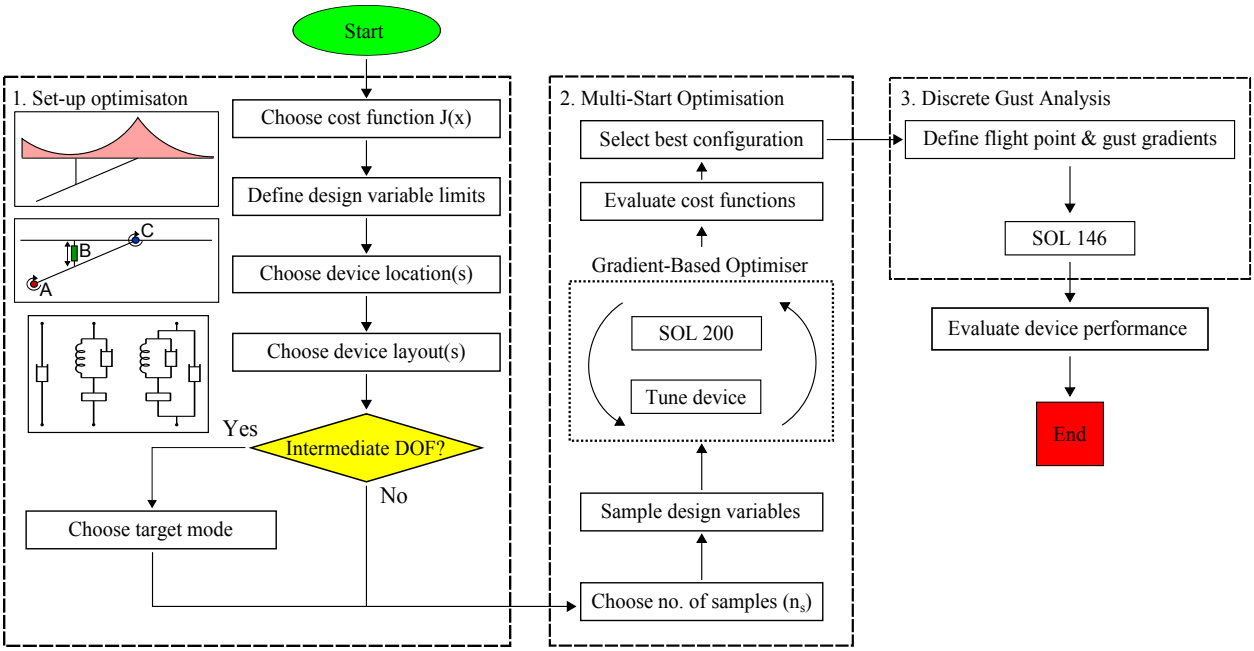

Fig. 3 Device optimisation process

expanded to include the new device DOF, $x^T = [x_s, x_d]^T$ where x contains the independent DOFs of the system which for MSC Nastran are the displacement of the nodes in the local coordinate system. The internal DOF introduces a new mode into the system which can be be tuned to match the frequency of one of the flexible modes of the host structure.

B. Device Optimisation Framework

Figure 3 shows a flowchart of a software framework for optimising a vibration suppression device which alleviates gust loads. For this study, the optimisation of the device is conducted using MSC Nastran's built-in optimisation and design sensitivity solution sequence SOL 200 [32] and the dynamic aeroelastic solution sequence SOL 146 [33] is used to simulate the gust response. SOL 200 is a mutlidisciplinary tool that allows optimisation of a set of model-based design variables subject to the response from a variety of analysis types such as: statics, normal modes and frequency response as well as static aeroelastic and aeroelastic stability (flutter). The main advantage of using SOL 200 is that it computes the gradients of response quantities with respect to the design variables analytically, meaning that the optimisation requires fewer function evaluations and consequently is much quicker than an algorithm that uses finite differences to estimate the gradients. This is an important consideration when applying the principles of mechanical network design to complex mechanical structures that can contain thousands or even millions of DOFs.

There are three main factors to consider when using SOL 200 to optimise a vibration absorber to alleviate gust loads:

- Continuous and discrete gust analysis are types of *dynamic aeroelasticity*, therefore, the optimisation of the aircraft response to turbulence encounters constitutes a *dynamic response optimisation*. Problems of this type will typically have global design spaces [34] and as SOL 200 uses a gradient-based optimiser it is not suitable for

solving this class of problem, therefore additional measures will be required to ensure that the design space is successfully traversed and a global optimum is found.

- The dynamic aeroelastic response solution, SOL 146, cannot be invoked within SOL 200, hence it is not possible to directly optimise the device parameters to minimise the gust response. Instead, an alternative cost function which is independent of the gust response must be used. Although it is possible to optimise the gust response of an aircraft using Fluid-Structure-Interaction methods [35] such an approach is not always favourable given the increased computational cost of dynamic aeroelastic analysis.
- SOL 200 can only cater for linear finite element models and linear analysis types, therefore, nonlinearities in the structure, aerodynamics or device properties will not be considered.

In order to mitigate for these points, the optimisation framework uses a *Multi-Start Optimsation* approach [36] to sample the multi-modal design space before running a local gradient-based optimisation at each sample point. The cost function is formulated in terms of a frequency response problem with the device parameters optimised to reduce the influence of certain modes of the structure that are identified as having a significant participation during the gust response. This approach is particularly useful for two reasons: Firstly, the optimisation of the device is decoupled from the gust response which removes the need to run a computationally expensive gust analysis for each function evaluation. Secondly, the lower computational cost means the approach can easily be applied to high-fidelity finite element models given the generic implementation via Nastran. This is an important consideration as the device properties will be tightly coupled to the mass and stiffness of the model which will vary significantly between a 3D and 1D model, even when a model reduction technique is employed. Further details on each module of the optimisation framework are provided in the following sections.

1. Setting up the optimisation

There are several stages involved in the set-up of the optimisation problem:

1) **Cost function.** The purpose of the device is to alleviate gust loads by reducing the participation of modes that have a significant contribution to the gust response. This can be achieved by adding damping to that mode or by tuning the device frequency to match the modal frequency, therefore, the cost function must be able to observe changes in a desired response quantity as a function of frequency, $X(\omega) = H(\omega)F(\omega)$ where,

$$H(\omega) = \left[K - \omega^2 M + i\omega C\right]^{-1}, \tag{2}$$

where X is some output response from the system, F is a vector of applied forces, H is the frequency response function (FRF) matrix, ω is the forcing frequency and the M, C, K matrices include the terms from the device. As the device will target gust loads it is sensible to evaluate the transfer function relating the beam loads and

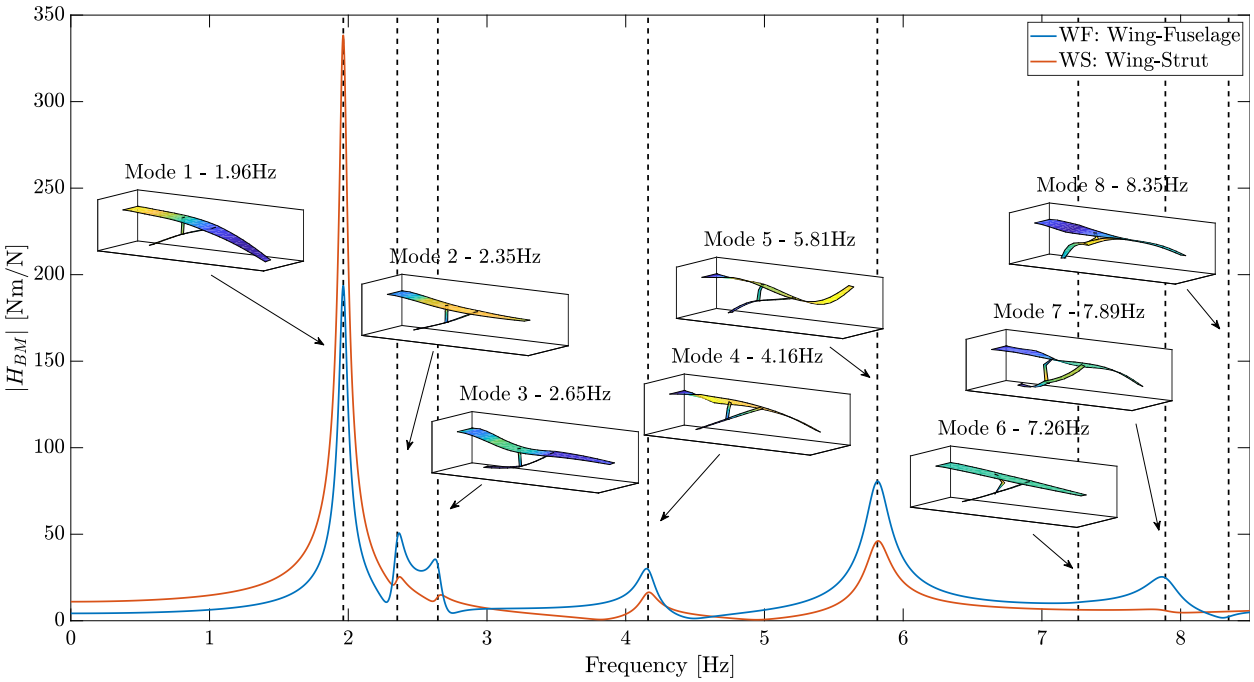

Fig. 4 Spanwise bending moment FRF due to a vertical harmonic force at the wing tip with 3% modal damping

responses. More specifically, the spanwise bending moment will be evaluated as it typically sizes the wing covers which constitute a significant portion of the wing weight. An example of this quantity is shown in Fig. 4 for the bending moment at the Wing-Fuselage (WF) and Wing-Strut (WS) joint for the case where no devices are included in the model; the first eight flexible modes are shown to highlight which mode contributes to the bending moment at these points in the wing. Note, there is no 'engine-mode' as the engine is included in the model as a lumped mass and there is no structural representation of the pylon. From Fig. 4 it is clear that the fundamental mode dominates the bending moment at the WS joint as the first mode corresponds to a 'flapping' motion of the outboard wing. However, the bending moment at the WF location includes contributions from the first five modes, so any device configuration that wishes to minimise loads at this point must be effective across multiple modes. Finally, the cost function is defined as the area under the transfer function, which for a discrete response and a suitably small frequency increment, is approximated by,

$$J_a(v) = \delta f \times \sum_{f_1}^{f_2} |H_{BM}(v, f)|, \tag{3}$$

where, v are the design variables, δf is the frequency increment, f is the frequency, f_1 and f_2 are the upper and lower limits of the frequency band and H_{BM} is the FRF matrix corresponding to the spanwise bending moment. This cost function has been chosen as it allows multiple modes to be targeted by careful selection of the upper and lower frequency limits which will be critical if there are multiple modes that the device must influence.

Table 4 Upper and lower bounds for the device parameters.

Design Variable	Lower Bound	Upper Bound	Translational Units	Rotational Units
Spring Stiffness	1	1×10^8	N/m	Nm/rad
Damping Coefficient	1	1×10^5	N/ms^{-1}	$Nm/rads^{-1}$
Mass Ratio	1×10^{-4}	0.1	–	–

2) **Design variables.** The design variables in this study are the device spring stiffness (k), damping coefficient (c) and inerter mass-ratio (μ). The mass-ratio is defined as a fraction of the primary structure mass, which for this study is the wing, including truss structure, with a total mass (M_{wing}) of 10467kg accounting for all primary and secondary structural masses. A maximum ratio of 10% has been chosen for μ, however, as an inerter element is used the actual mass of the device will be far less than 10% of the wing mass. For instance, a typical value of the inertance-to-mass ratio is around 40-80, see for example the commercially available device tested in Gonzalez-Buelga *et al.* [37], although devices have been produced with ratios as high as 300 [18]. An upper limit of 1×10^5 is chosen for c as this has been shown in previous studies to provide moderate loads alleviation [38] and an upper limit of 1×10^8 is defined for k as this covers device tuning frequencies up to 50Hz when considering the maximum permitted inertance value. A summary of the design variable upper and lower bounds is provided in Table 4.

3) **Device location(s).** It is hypothesized that any joint-location between the wing and truss-structure will experience some level of relative motion thereby providing a possible location for the two terminal device. As the truss topology is fixed for this study the device position is constrained to the three candidate locations shown in Fig. 5, these are the hinge joints at the root and tip of the strut as well as a device in parallel with the jury-strut. The hinge connections at the root and tip of the jury-strut are not considered as the primary load path for the jury-strut is tension/compression for which a translational device is best suited. The study in Sections IV and V will consider both a single device or a combination of devices at any of these three locations.

4) **Device layout(s).** As this research is concerned with establishing the viability of a vibration suppression device as a method for gust loads alleviation (GLA) in TBW a component layout to the device is assumed, i.e. adopting a *structure-based* approach [28]. This assumes a fixed layout device, within which each mechanical element is

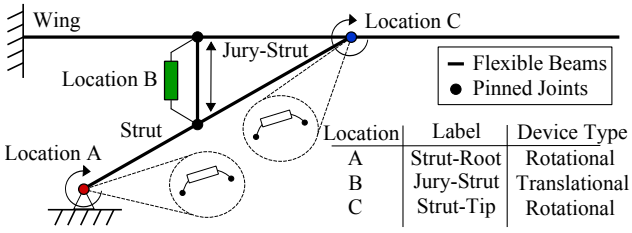

Fig. 5 Schematic of a TBW showing the three candidate device locations.

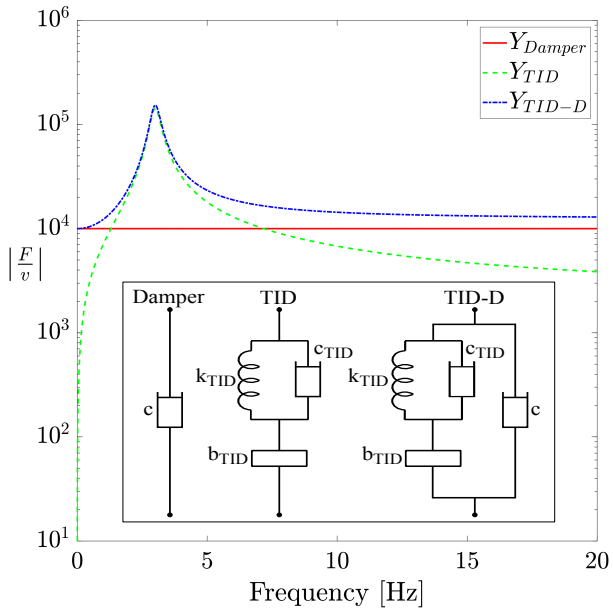

Fig. 6 Force-Velocity transfer functions inset with the three candidate layouts for the case where $b_{TID} = 1000kg$, $c_{TID} = 2500N/ms^{-1}$, $k_{TID} = 35,531N/m$ and $c = 10,000N/ms^{-1}$.

optimised to improve the performance. Here, three device layouts are considered:

1) **Damper** - A linear, viscous damper is considered to be the simplest vibration suppression device and will provide a suitable baseline for evaluating other device configurations.
2) **Tuned-Inerter-Damper (TID)** - The TID [22] is analogous to the classical Tuned-Mass-Damper (TMD) with the exception that the mass element is replaced by an inerter, as in Fig. 6.
3) **Tuned-Inerter-Damper-Damper (TID-D)** - Similar to the TID but with a damper in parallel.

Figure 6 shows the force-velocity transfer function, Y, as well as the layouts for the three devices considered. In contrast to the damper which has a constant value across all frequencies, the TID and TID-D devices can target a particular frequency by selecting the inertance and stiffness values appropriately. The exact tuning condition of the device is dependent on the background effects of the host structure [31], however the formula $\omega = \sqrt{k/b}$ can be used to place the device in the correct region of the frequency domain before the optimiser tunes the device. The advantages of a TID device over the conventional TMD are twofold: Firstly, the use of the inerter element allows a force to be imparted at both terminals of the device, something that is particularly useful for the TBW configuration as it allows for the possibility of a device that can influence multiple parts of the structure. Secondly, the inerter can provide an inertance which is far greater than the mass of the device, this has obvious benefits in an aerospace application as the weight of the aircraft should be kept to a minimum.

2. Multi-Start Optimisation

The multi-start method involves sampling the design space at an appropriate number of intervals so as to ensure the many local-minima are captured. Next, a gradient-based optimiser, in this case the Modified Method of Feasible Directions algorithm belonging to MSC Nastran's MSCADS suite of optimisers within SOL 200, is used to search the local design space for an optimal solution at every sample point. Once all samples have been evaluated the minimum cost function and its associated design variables are selected from the individual optimisation results. Whilst this approach allows global design spaces to be traversed it is important to note that it does not guarantee a global optimum. Also, the robustness of the solution is heavily dependent on the initial sampling of the design space [39].

In this study the Latin Hypercube Sampling (LHS) algorithm `lhsdesign` is used to randomly sample each design variable. A parameter study was carried out to determine the number of samples (n_S) and a value of 100 was chosen as this was found to give consistent results. As some of the design variables have allowable values that span several orders of magnitude the sample points from `lhsdesign` are mapped to an exponential distribution to ensure the design space is sufficiently covered.

Next, the optimisation process is called n_s times with each run using a new sample point as the initial conditions, however, before SOL 200 is executed a check is made on the device layout. If a TID or TID-D layout has been selected and a tuning mode specified then the initial device stiffness is adjusted using the approximate tuning rule introduced in Section II.B.1

$$k = \mu \times M_{wing} \times \omega^2, \tag{4}$$

Once the optimisation loop has finished the best design associated with the minimum cost function value across all sample points is extracted and the necessary bulk data entries are passed into the gust analysis module.

3. Discrete Gust Analysis

MSC Nastran SOL 146 is used to compute the transient gust response of the aeroelastic model. SOL 146 is a frequency domain solution that uses modal coordinates u_h to solve an equation of the form,

$$\left[-M_{hh}\omega^2 + iC_{hh}\omega + (1+ig)K_{hh} - \frac{1}{2}\rho V^2 Q_{hh}(m,k)\right]\{u_h\} = \{P(\omega)\}, \tag{5}$$

where subscript hh denotes the modal set, g is the structural damping parameter, ρ is air density, V is the aircraft forward velocity, Q is the matrix of aerodynamic influence coefficients (AIC) which is a function of Mach number m and reduced frequency k, and P is the generalised frequency domain loading. The AIC matrix is determined using Doublet Lattice Method (DLM) aerodynamic theory and the applied frequency load is calculated from the Fourier Transform of the

time-domain gust loading. In this study only discrete gust loadings in the form of "1-cosine" gusts [40] are considered,

$$w_g(t) = \frac{U_{ds}}{2}\left[1 - cos\left(\frac{\pi V t}{H}\right)\right], \tag{6}$$

where w_g is the gust vertical velocity, H is the gust gradient (distance to reach the peak gust velocity), V is the aircraft forward velocity in TAS and U_{ds} is the gust design velocity, defined as

$$U_{ds} = U_{ref} F_g \left(\frac{H}{106.17}\right)^{\frac{1}{6}}, \tag{7}$$

where F_g is the flight load alleviation factor and U_{ref} is the reference gust velocity in EAS, varied linearly from 13.4m/s EAS at 15,000ft to 7.9m/s EAS at 50,000ft as specified in CS-25 [40].

III. Gust Response of the Baseline Aeroelastic Model

Before a device optimisation study can take place it is necessary to determine the baseline gust response of the aeroelastic model so that the effect of the vibration suppression device(s) can be quantified.

To generate the loads envelope ten equally-spaced gust gradients are considered in the range 9m to 107m and for each gust response the maximum beam loads are calculated across all time steps for every beam node along the wing, strut and jury-strut. The simulation is carried out at the SUGAR Volt cruise flight point of 36,000ft at Mach = 0.75 [7] which, using the equations in Section II.B.3, yields a gust reference velocity and flight load alleviation factor of 10.12m/s EAS and 0.98 respectively. Solution frequencies up to 30Hz are included and a frequency increment of 0.005Hz is used.

The incremental spanwise bending moment is used to evaluate the baseline gust response and benchmark the performance of the device as these loads tend to be critical for sizing the wing box cover thickness which forms a major component of the wing structural mass. Note that in a commercial sizing process the full loads envelope would be constructed by correlating all six beam loads as a function of time in order to determine the true maximum and minimum loads [41], however, for the sake of brevity only the spanwise bending moment is considered so as to demonstrate the loads alleviation potential of a two-terminal vibration suppression device.

Figure 7 shows the incremental gust loads envelope for the spanwise bending moment along the wing with colour-coded markers indicating which gust gradients are driving the loads at the different spanwise locations. Inspecting Fig. 7 it is clear that a number of gusts are responsible for generating the wing bending moment envelope, implying that any device that seeks to minimise gust loads must be effective across the entire gust spectrum. There are two spanwise locations where the bending moment reaches a maxima, these are the strut-attachment point and the wing-fuselage joint. This suggests that a device that can reduce the loads at one or both of these points will provide a net benefit to the wing gust response and may also minimise the wing weight via reduction of the critical loads envelope.

One of the key requirements of the device optimisation process is to understand which modes the device must target in order to minimise the chosen cost function. Figure 8 shows the maximum modal coordinate for the first seven structural modes as a function of gust gradient and plots of the corresponding modeshapes can be found inset in Fig. 4. It shows that the dominant mode in the gust response is the fundamental mode, which corresponds to an outboard wing 'flapping' mode. The other modes follow, almost in mode order, with some fluctuation at the lower and higher ends of the gust spectrum, although there is a clear gap between modes two and three and the rest of the modes.

The dominance of the low frequency modes is due to the frequency and power content of the gust input signal. Examining Fig. 9 it is clear that the gust bandwidth drops sharply as the gust gradient increases whilst the gust power increases in a logarithmic fashion. The effect of this is that the low frequency modes receive a much higher input power than the high frequency modes, meaning that these modes participate more in the gust response. Also, Fig. 9 shows that the maximum gust bandwidth within the CS-25 mandated limits is approximately 8.7Hz, however, that is not to say that higher frequencies should not be accounted for when simulating the gust response. The gust bandwidth simply gives an indication of which parts of the frequency spectrum are most important during a gust encounter, thereby focusing the efforts of a vibration suppression device.

In summary, the incremental spanwise bending moment envelope reveals two locations along the wing where the loads reach a maximum; these are the wing-strut joint and the wing-fuselage joint. These locations will be used as the basis of the cost function and also to evaluate the performance of the device by comparing the value of the loads at these locations with different device configurations. Figure 8 has shown that the lower frequency modes are most active throughout the gust spectrum and constitute the main components of the structural response. Also, from Fig. 9 it is clear that for the chosen flight point all one-minus cosine gusts have a bandwidth lower than 8.7Hz, therefore

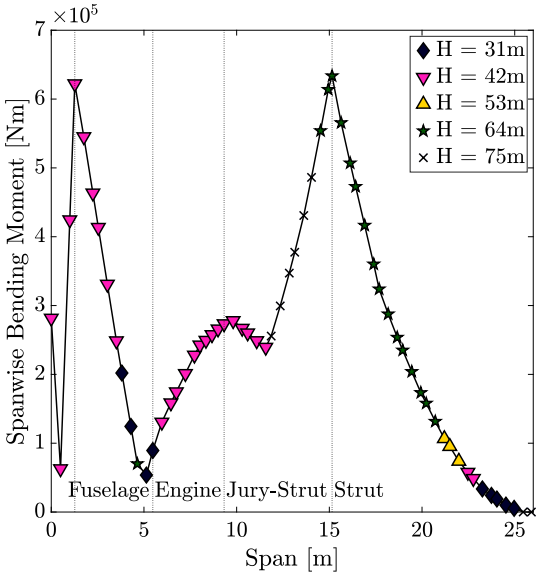

Fig. 7 Incremental gust loads envelope for the wing spanwise bending moment

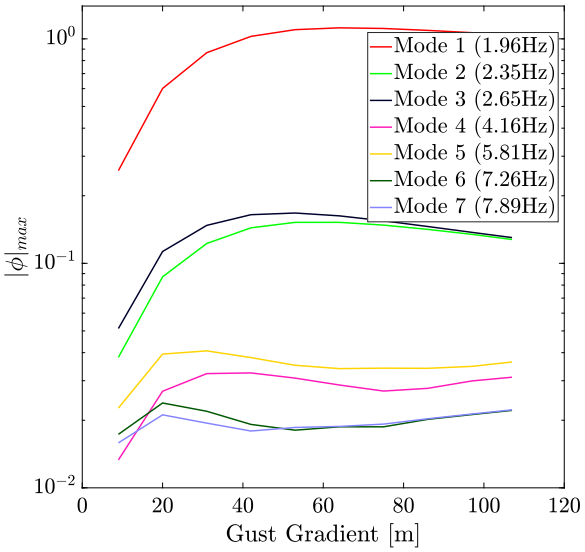

Fig. 8 Maximum modal coordinate for the first seven modes as a function of gust gradient

it is appropriate for the vibration suppression device to target the low frequency modes in order to influence the gust response and reduce loads.

IV. Passive Gust Loads Alleviation Using a Single Device

The purpose of this section is to determine which device layout is most appropriate for reducing gust loads when only a single device is considered. This is achieved by running two optimisation studies: the first considers a single damper placed at one of the candidate locations and the second extends this study to all three device layouts.

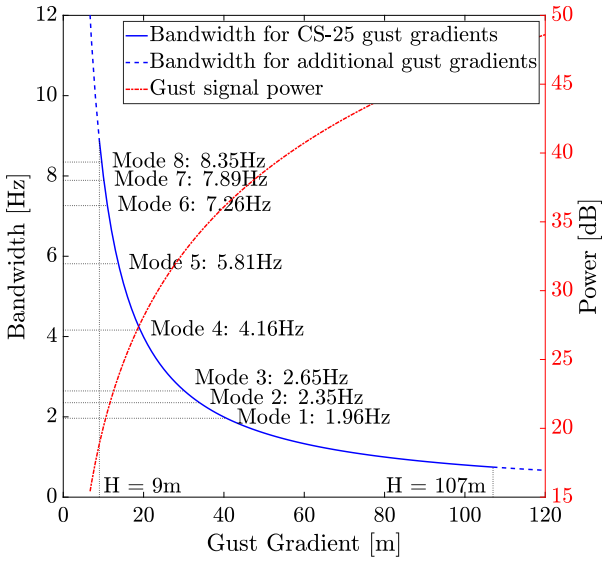

Fig. 9 Gust bandwidth and power as a function of gust gradient

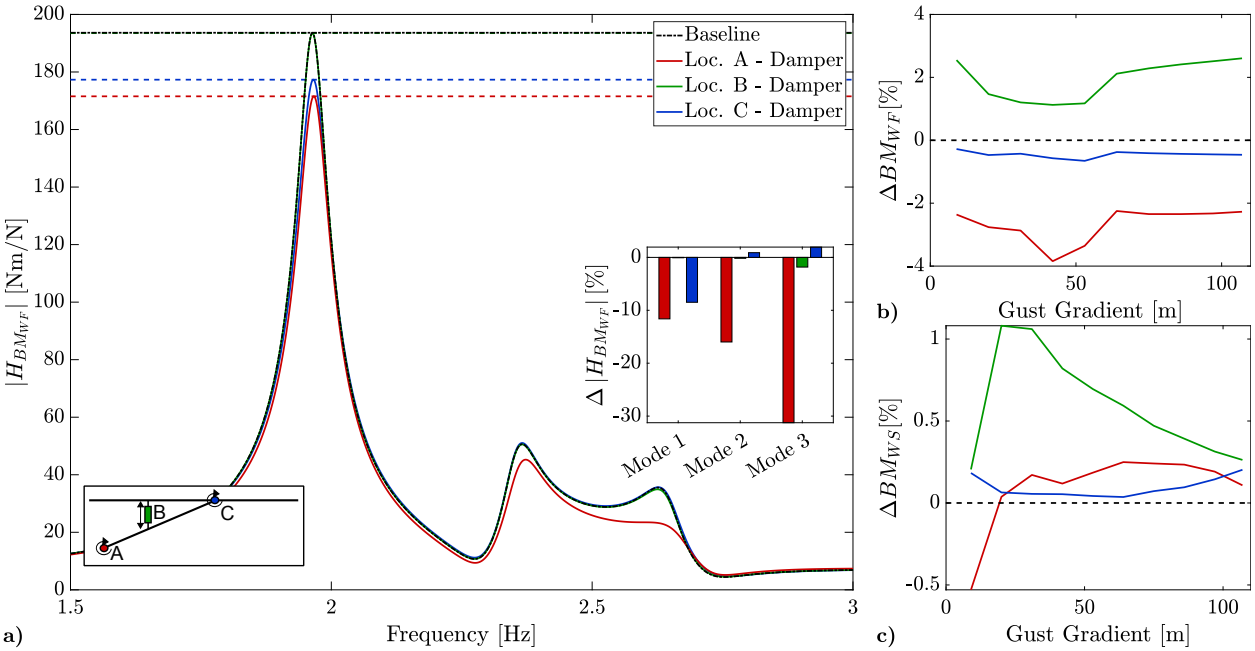

Fig. 10 Gust loads alleviation results for the case with a damper at locations A, B and C.

Table 5 Cost function values and device parameters for the case with a damper at locations A, B and C.

Location	Layout	c	$\Delta J_a(v)$	min(ΔBM_{WF})	mean (ΔBM_{WF})
A	Damper	100,000	-5.39%	-3.84%	-2.67%
B	Damper	17,253	-0.22%	1.20%	1.94%
C	Damper	45,385	-0.80%	-0.65%	-0.45%

A. Gust Load Alleviation Using a Single Damper

Employing a single damper, the viscous damping coefficient of the device is optimised in order to reduce the area under the wing-root bending moment transfer function, $J_a(v)$, at the wing-fuselage joint location. The wing-fuselage location is chosen as it captures the response of multiple modes, as opposed to the wing-strut FRF which is mostly the fundamental mode. Figure 10a shows the baseline and optimised transfer function for the three different damper locations as well as the change in FRF amplitude at the original natural frequencies. Figures. 10b and 10c show the percentage change in the actual gust-induced maximum spanwise bending moment as a function of gust gradient for the wing-fuselage joint and wing-strut attachment points respectively. Note that as the difference is presented with respect to the baseline aeroelastic model a negative value indicates that the device has a beneficial effect, whereas a positive value is detrimental. Table 5 shows a summary of the device performance and damping coefficients for each of the three locations.

The results show that placing a damper at Location A achieves the lowest cost function value. In terms of the frequency domain performance, the damper has successfully reduced the FRF response amplitude around modes two

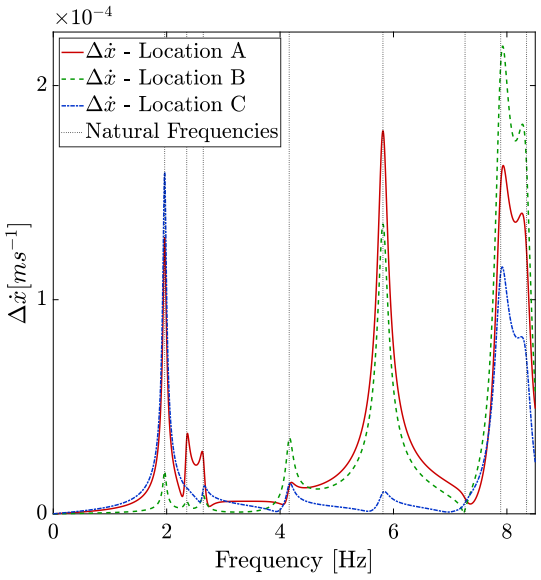

Fig. 11 Relative velocity across device terminals for each candidate location in response to a unit harmonic load applied in the positive z-direction at the wing-tip.

and three as well as a reduction around mode one. This has translated into a consistent reduction in spanwise bending moment at the wing-fuselage joint across all gust gradients considered with a maximum change of 3.84% for the 42m gust, however, this is at the expense of a very large viscous damping coefficient. Interestingly, the small amount of additional damping that has been provided by the damper around mode one has a negligible effect on the loads at the wing-strut joint, despite mode one having the largest contribution to the loads at this wing position.

The damper at location B has had a negligible effect on the amplitude of the first three modes and has increased the spanwise bending moment at both monitoring points for all gust gradients considered. It is hypothesized that this is because the force generated by the damper acts in the same plane as the lift force acting on the wing, which leads to an increase in sectional shear force in the region around the jury-strut and a subsequent increase in spanwise bending moment at nodes away from the jury-strut attachment point. For this reason, a device in parallel with a vertically-orientated jury-strut may be inappropriate for reducing the wing bending moment. Conversely, the damper at location C has provided additional damping to the fundamental mode but has had very little effect elsewhere and has only had a minor effect on the on the bending moment values at the monitoring points. For the wing-fuselage joint there is a net reduction in bending moment, although it is modest - the maximum reduction is 0.65%. There is a net increase in bending moment at the wing-strut joint but it does not exceed 0.2%, which may be acceptable once static aeroelastic load cases are considered. This suggests that modes two and three are driving the value of the wing-fuselage bending moment and that targeting these modes will lead to a much larger reduction in loads.

The tendency for a device at a particular location to influence the response of certain modes is suggested by considering the relative velocity across the device terminals as a function of frequency. Examining Fig. 11, it is clear that

location A is best suited to targeting the response of the first three modes due to the increased relative angular velocity at low frequencies, whereas location B is more appropriate for the higher frequency modes as these are dominated by truss bending and twist modes. Interestingly, location C experiences significant relative velocity for the fundamental mode. This is a direct consequence of the pinned connection between the primary strut and the wing which allows the outboard section of the wing to 'flap' freely about this joint and generate large bending moments at the joint location.

In summary, this study has shown that a damper positioned at location A using the highest permitted viscous damping coefficient can achieve a maximum reduction of 3.84% in spanwise bending moment at the wing-fuselage joint. Furthermore, the favourable influence of the damper is due to the increased modal damping of the first three structural modes, indicating that for a device to successfully reduce gust loads it must target each of these modes. For the other damper locations, location B results in a net increase in spanwise bending moment whilst a damper at location C provides only a minor benefit via increased damping for the fundamental mode. In all instances there was a negligible change in loads at the wing-strut joint with the change in bending moment restricted to ±0.5%. All dampers required a large viscous damping coefficient to have an effect on the gust response but without considering the design of the damper it is not possible to say whether these values are realistic or not. Finally, given the poor gust load alleviation results as well as the reduced relative velocity across the device terminals for the first three modes, location B will not be considered in further studies.

B. Gust Load Alleviation Using a Single TID or TID-D

In this section the TID and TID-D layouts are compared for the case where a single device is used in either location A or location C and the results in this section are benchmarked against the damper performance from Section IV.A. Note, as the study in the previous section has shown that reducing the response of the first three modes is important for alleviating gust loads the cut-off frequency f_2 is set to 5Hz to prevent the device targeting the higher frequency modes that are less critical to the gust response.

A preliminary study was conducted to determine the effect of initially tuning each device to one of the structural modes before running the optimisation. It was found that for a TID device at location A setting the initial tuning mode, m_{dev}, to the third structural mode yielded the best possible GLA and for both the TID and TID-D devices, whilst at location C the best GLA was obtained when the device was tuned to the fundamental mode; although in both cases the performance was inferior to the pure damper case at the respective locations. The case with a TID-D at location A was found to be insensitive to the initial device tuning frequency as the optimiser converged to the same optimum solution regardless of initial conditions, furthermore the performance of the TID-D was superior to the pure damper. A selection of these results are shown in Fig. 12 and their respective performance metrics and device parameters are given in Table 6.

Considering the devices at location A, the TID has successfully reduced the FRF amplitude for modes two and three

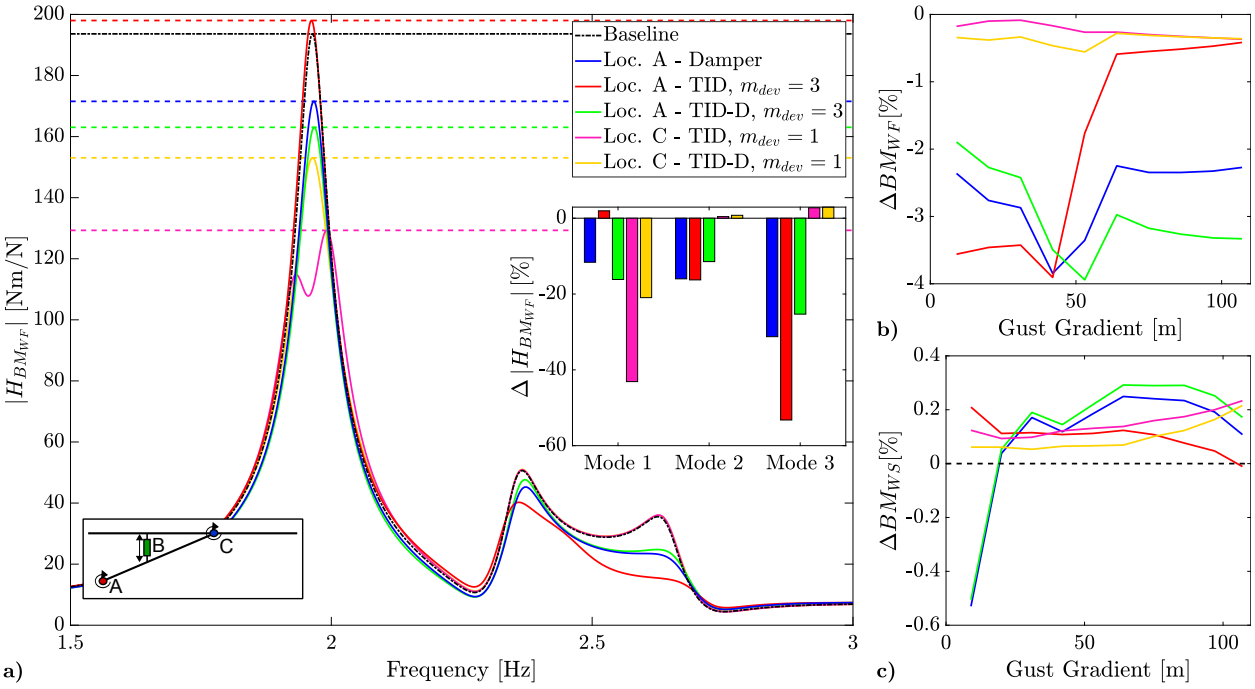

Fig. 12 Gust loads alleviation results for a selection of single device configurations.

Table 6 Cost function and device parameters for the device configurations in Fig. 12

Location	Layout	c	μ	c_{TID}	k_{TID}	m_{dev}/f_{TID}	$\Delta J_a(v)$	min(ΔBM_{WF})	mean (ΔBM_{WF})
A	Damper	100,000	-	-	-	-/-	-5.39%	-3.84%	-2.67%
A	TID	-	0.10	1425	3.46×10^5	3/2.87	-2.13%	-3.91%	-1.87%
A	TID-D	100,000	0.10	1	2.09×10^5	3/2.23	-6.03%	-3.94%	-3.01%
C	TID	-	0.075	84.20	1.40×10^5	1/2.10	-2.63%	-0.37%	-0.24%
C	TID-D	17178	0.081	1005.2	1.61×10^5	1/2.17	-1.97%	-0.56%	-0.37%

with a small increase in the response of mode one. This has translated into a reduction of almost 4% in BM_{WF} for the shorter gust lengths but during longer gusts the benefits are lessened as these gusts are dominated by the response of the fundamental mode. This is a clear consequence of the TID targeting mode three which resulted in an increased response of mode one. The TID-D is able to mitigate against this by providing damping to those modes which are not targeted by the TID, yielding a more consistent reduction in loads across all gust gradients which serves to highlight the importance of using a cost function and device layout that can target multiple structural modes.

For location C, the optimiser has tuned the TID to match the frequency of the fundamental mode, clearly demonstrated by the 'split-peak', enabling the device to significantly reduce the amplitude of mode one, although modes two and three are unaffected. The TID-D device has had a less pronounced effect on the fundamental mode and the split peak is no longer present due to the increased damping from the parallel damper. In terms of GLA, the TID-D has achieved a better reduction in gust loads despite having a lower cost function value, which is clear evidence that the mapping

between the optimised FRF and the gust response is not direct. Furthermore, the GLA performance of both devices at location C is inferior to the devices at location A because the response of modes two and three are not influenced by a device at location C due to the reduced relative velocity at these locations/modes.

For all device locations and layouts there is a negligible effect on the spanwise bending moment at the wing-strut joint. This may be because the input power to this mode is simply too great for the device to have a significant impact on the participation of this mode without generating an extremely large force in order to influence the outboard motion of the wing. Even so, as the change in loads is ±0.5% this is an acceptable outcome.

There is a significant variation in the optimum device parameter values for the different device layouts. When the TID is used the damping coefficient is much lower than the pure damper case, which shows the benefit of implementing a tunable device over the pure damper case, however the TID-D device has the opposite configuration. That is, the parallel damper element has a very large damping coefficient whilst the damper within the TID is effectively zero as it is at the lower bound of the design variable. In this case the addition of the TID yields only a small reduction in gust loads, although, it does improve the performance during the longer, low-frequency, gusts which is achieved by the TID element targeting the response of mode one. In terms of inertance values both the TID and TID-D have opted for the maximum possible mass ratio. This is consistent with the fundamental theory of vibration absorbers which states that a higher mass ratio increases the separation between the split-peak frequencies and provides a broader bandwidth for the device which then manifests itself as a reduction in the overall area under the FRF curve.

In summary, the studies presented in this section have shown that it is possible to achieve a maximum reduction in wing-fuselage bending moment of 3.94% using a single device configuration. The best performance was achieved by the TID-D layout but in general either a damper, TID or TID-D device can provide a reasonable reduction in gust loads when it is positioned at location A. For a device location C, a small reduction in loads of the order of 1% is achievable and location B was found to be unsuitable due to the reduced relative velocity across the jury-strut terminals for the lower frequency modes.

V. Gust Loads Alleviation Using Two Devices

In the previous section it was shown that it is possible to reduce gust loads by using a device to target specific structural modes, however, as the tunable device layouts considered in this paper only have one internal degree-of-freedom it is not possible to target more than one mode with a single device. To mitigate this, a two-device configuration will be investigated which allows two devices to simultaneously target different structural modes. Based on the relative velocity FRF in Fig. 11, a pair of devices located at the strut-root joint and at the strut-tip joint should be sufficiently active during the first three modes. Also, the results in the previous section have shown that a tunable device is the best option for influencing a specific mode, therefore, a pair of TID-D devices will be placed at location A and location C and as with the previous study f_2 is set to 5Hz to minimise the response of the first three modes.

Figure 13 shows the gust loads alleviation results for the two device configuration and Table 7 details the parameter values and the performance metrics. Examining Fig. 13b, it is clear that the two device configuration has achieved a greater reduction in spanwise bending moment at the wing-fuselage joint, with a maximum change in bending moment of -4.19% and an average change of -3.37%. While still relatively small, both metrics are better than any of the single device configurations considered in Section IV.B. Also, despite the increased damping at mode one there is still a negligible change in the loads at the wing-strut joint which is consistent with the results from Section IV.

Also shown in light grey on Fig. 13 is the undamped FRF for the two device configuration. This highlights the two new modes that have been introduced by the tunable devices and provides a clear indication of the classical split-peak behaviour of the vibration absorbers. The TID-D at location A has tuned to the fundamental mode whilst the TID-D at location C has targeted mode three, both of which are expected given the increased relative velocity at the respective device locations. Furthermore, this result clearly demonstrates the ability of a combined FE/optimisation approach to tune an inerter-based device attached to a complex host structure without the need to adopt tuning rules, such as those proposed in [31], allowing for the possibility of more complex device layouts to be investigated which could yield greater GLA benefits.

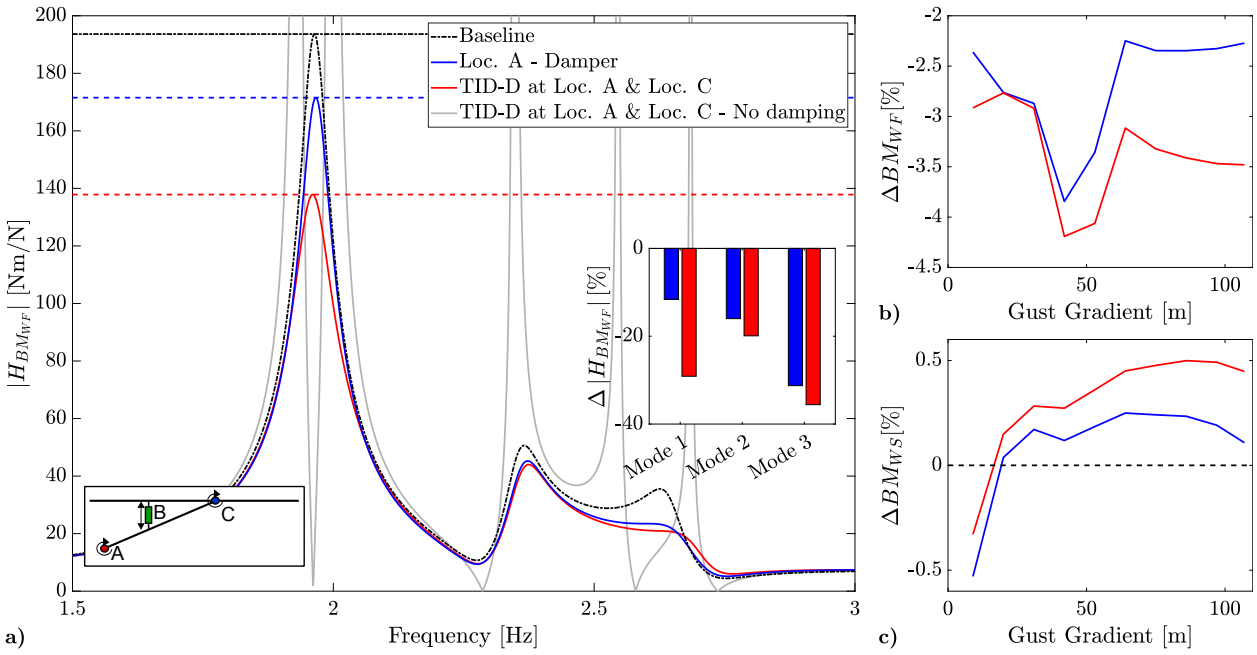

Fig. 13 Gust loads alleviation results for the two device configuration.

Table 7 Cost function and device parameters for the two device configuration

Location	Layout	c	μ	c_{TID}	k_{TID}	m_{dev}/f_{TID}	$\Delta J_a(v)$	min(ΔBM_{WF})	mean (ΔBM_{WF})
A	TID-D	100,000	0.10	1	3.38×10^5	3/2.83	-7.98%	-4.19%	-3.37%
C	TID-D	68.60	0.08	1,230	1.64×10^5	1/2.19			

Concerning the parameter values, the TID-D at location A has opted for the maximum damping coefficient value for the parallel damper whilst the TID element has tuned itself to mode three with a minimum damping coefficient. The TID-D at location C has an almost negligible damping coefficient for the parallel damper which implies that the vibration absorber effect is more beneficial than the modal damping. The TID element has a moderate value of damping coefficient and has tuned itself to the first structural mode. These results were largely expected given the increased relative velocity at the respective device locations, as shown in Fig. 11.Finally, Fig. 14 shows a comparison between the baseline wing incremental gust loads envelope and the case where the structure is augmented with a TID-D at locations A and C. All six beam loads are presented to show that even though the optimisation process only considered the spanwise bending moment at the wing-fuselage joint, as the targeted modes are global quantities, the device configuration has successfully reduced the loads across the span of the wing. Specifically, for all six beam loads there is a reduction of approximately 4% for spanwise stations inboard of the strut-attachment point. Clearly, if if gust loads are critical for the components in the wing then a 4% reduction in loads will translate to a reduction in the wing weight, this indicates the

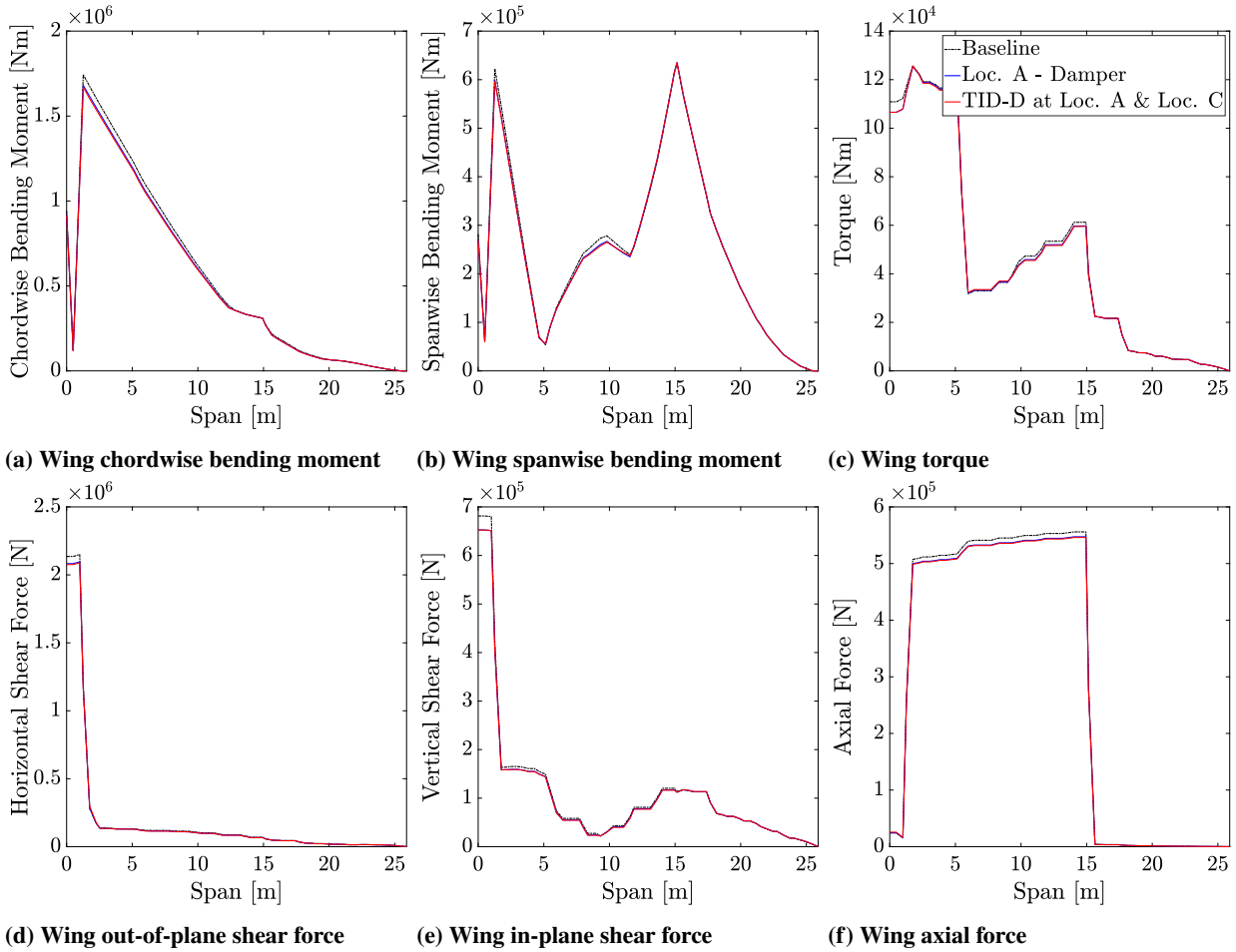

(a) Wing chordwise bending moment **(b) Wing spanwise bending moment** **(c) Wing torque**

(d) Wing out-of-plane shear force **(e) Wing in-plane shear force** **(f) Wing axial force**

Fig. 14 Incremental gust loads envelope for the wing beam loads, comparing the baseline model and the two device configuration

scale of performance benefits that might be realised from passive devices installed on a high aspect-ratio braced wing. Designing a device that could fulfill multiple functions would help mitigate for the fact that the device is a fixed mass that would need to be carried for the duration of the mission. For example, another potential application of the device is alleviating wing flutter. Analysis carried out as part of the NASA/Boeing SUGAR project [7] indicated that wing flutter was a combination of wing and strut bending, implying that a passive vibration suppression device could be used to alleviate flutter so long as the flutter modeshapes have translational or rotational components at the device locations. Furthermore, the loads reduction provided by the device could be translated into an improvement in fatigue life by using an analytical fatigue model such as the one proposed in [42]. However, as the purpose of this study is to introduce the concept of using vibration suppression devices to provide gust loads alleviation, any benefit in terms of fatigue life extension is considered beyond the current scope.

As a vibration suppression device is a novel and unusual design feature in a fixed wing aircraft there are likely to be many technical challenges to the certification of this technology, however, because of this novelty, the requirements are not explicitly defined in any of the existing certification documents - although discussion on the use of "Passive Flutter Dampers" is provided in Section 5.1.4.3 of [40]. Such devices are concerned with suppressing control surface flutter and not providing gust loads alleviation however the requirements in [40] can be used as guidelines. For example, the probability of device failure would need to be assessed, especially for the case where multiple devices are included, and a fail-safe design methodology would need to be adopted, similar to the approach taken in reference [43]. Here, the strength and stability of the airframe must be guaranteed even for conditions where the device had failed. Furthermore, the capabilities of the passive system would have to be demonstrated in wind tunnel tests and associated analysis models validated. Inspiration could also be taken from the rotorcraft industry where blade lead-lag dampers have been designed and certified for a number of helicopters [15] and anti-vibration control systems have been installed on the EuroCopter EC225 [44] and EC130T2 [45].

VI. Conclusions

This paper has presented a novel method for gust loads alleviation in a truss-braced wing based on using vibration suppression devices to target the specific modes of the structure in order to reduce their participation in the gust response. Three candidate locations were considered, the two hinge locations at the root and tip of the primary strut and the jury-strut, and three device layouts have been tested, a pure damper and two inerter-based devices known as the Tuned-Inerter-Damper and the Tuned-Inerter-Damper-Damper. The gradient-based optimiser within MSC Nastran™ Solution 200 was used to optimise the device parameter values and a multi-start optimisation approach was used to traverse the global design space and find a suitably global solution.

The results indicated that the frequency-response optimisation approach introduced in this paper allows a vibration suppression device to be designed that is capable of providing moderate loads relief across the gust spectrum.

Furthermore, for the half-wing model considered it was found that the strut-root joint was the best location for a device regardless of the device layout, whilst the strut-tip joint provided only minor loads relief and a device located parallel to the jury-strut was unsuitable for gust loads alleviation. Considering the device layout, for the case where a single device was considered a damper at the strut-root joint achieved a maximum reduction of 3.8% in spanwise bending moment at the wing-fuselage joint, however this was at the expense of a very large viscous damping coefficient. In contrast, the use of an inerter-based device enabled similar reductions in incremental gust loads with only a fraction of the viscous damping coefficient. When two inerter-based devices were considered there was a slight increase in gust load alleviation with a maximum reduction of 4.2% in spanwise bending at the wing-fuselage joint and similar reductions inboard of the strut-wing joint for the other five beam loads. Furthermore, the results have shown that for both the single and multiple device cases the optimised inerter-based devices have large mass ratios, although it was proposed that this could be mitigated by designing the device to have a large inertance-to-mass ratio in order to keep the actual mass of the device to a minimum.

Finally, this paper has demonstrated an approach for modelling and optimising a vibration suppression device attached to a generic finite element model. The use of MSC Nastran™ means that any generic finite element model and vibration suppression device can be considered, increasing the scope for the discipline of mechanical network design to be applied to a variety of large-scale problems.

Funding Sources

This research was funded by the UK Aerospace Technology Institute Agile Wing Integration (AWI) project (TSB-113041). Simon A. Neild was supported by an EPSRC Fellowship (EP/K005375/1) and Jason Z. Jiang is supported by an EPSRC grant (EP/P013456/1).

References

[1] Graham, W., Hall, C., and Morales, M. V., "The potential of future aircraft technology for noise and pollutant emissions reduction," *Transport Policy*, Vol. 34, 2014, pp. 36–51. doi:https://doi.org/10.1016/j.tranpol.2014.02.017.

[2] Gundlach, J. F., Philippe-André, Tétrault, Gern, F. H., Nagshineh-Pour, A. H., Ko, A., Schetz, J. A., Mason, W. H., Kapania, R. K., Grossman, B., and Haftka, R. T., "Conceptual design studies of a strut-braced wing transonic transport," *Journal of aircraft*, Vol. 37, No. 6, 2000, pp. 976–983. doi:https://doi.org/10.2514/2.2724.

[3] Meadows, N. A., Schetz, J. A., Kapania, R. K., Bhatia, M., and Seber, G., "Multidisciplinary design optimization of medium-range transonic truss-braced wing transport aircraft," *Journal of Aircraft*, Vol. 49, No. 6, 2012, pp. 1844–1856. doi:https://doi.org/10.2514/1.C031695.

[4] Carrier, G., Atinault, O., Dequand, S., Hantrais-Gervois, J., Liauzun, C., Paluch, B., Rodde, A., and Toussaint, C., "Investigation

of a strut-braced wing configuration for future commercial transport," *28th Congress of the International Council of the Aeronautical Sciences*, ICAS Bonn, 2012, pp. 2012–1.

[5] Mallik, W., Kapania, R. K., and Schetz, J. A., "Effect of flutter on the multidisciplinary design optimization of truss-braced-wing aircraft," *Journal of Aircraft*, Vol. 52, No. 6, 2015, pp. 1858–1872. doi:https://doi.org/10.2514/1.C033096.

[6] Bradley, M. K., and Droney, C. K., "Subsonic Ultra Green Aircraft Research: Phase I Final Report," Tech. rep., NASA, CR-2011-216847, 2011. URL https://ntrs.nasa.gov/search.jsp?R=20110011321.

[7] Bradley, M. K., Droney, C. K., and Allen, T. J., "Subsonic Ultra Green Aircraft Research. Phase II-Volume I; Truss Braced Wing Design Exploration," Tech. rep., NASA, CR-2015-218704, 2015. URL https://ntrs.nasa.gov/search.jsp?R=20150017036.

[8] Karpel, M., "Design for active flutter suppression and gust alleviation using state-space aeroelastic modeling," *Journal of Aircraft*, Vol. 19, No. 3, 1982, pp. 221–227. doi:https://doi.org/10.2514/3.57379.

[9] Bradley, M. K., Allen, T. J., and Droney, C., "Subsonic Ultra Green Aircraft Research: Phase II-Volume III; Truss Braced Wing Aeroelastic Test Report," Tech. rep., NASA, CR-2015-218704, 2014. URL https://ntrs.nasa.gov/search.jsp?R=20150017040.

[10] Bartels, R. E., Stanford, B., and Waite, J., "Performance Enhancement of the Flexible Transonic Truss-Braced Wing Aircraft Using Variable-Camber Continuous Trailing-Edge Flaps," *AIAA Aviation 2019 Forum*, 2019, p. 3160. doi:https://doi.org/10.2514/MAVIAT19.

[11] Livne, E., "Aircraft active flutter suppression: State of the art and technology maturation needs," *Journal of Aircraft*, Vol. 55, No. 1, 2017, pp. 410–452. doi:https://doi.org/10.2514/1.C034442.

[12] Castrichini, A., Siddaramaiah, V. H., Calderon, D., Cooper, J., Wilson, T., and Lemmens, Y., "Preliminary investigation of use of flexible folding wing tips for static and dynamic load alleviation," *The Aeronautical Journal*, Vol. 121, No. 1235, 2017, pp. 73–94. doi:10.1017/aer.2016.108.

[13] Stodieck, O., Cooper, J. E., Weaver, P., and Kealy, P., "Optimization of tow-steered composite wing laminates for aeroelastic tailoring," *AIAA Journal*, Vol. 53, No. 8, 2015, pp. 2203–2215. doi:https://doi.org/10.2514/1.J053599.

[14] Wlezien, R., Horner, G., McGowan, A., Padula, S., Scott, M., Silcox, R., and Simpson, J., "The aircraft morphing program," *39th AIAA/ASME/ASCE/AHS/ASC Structures, Structural Dynamics, and Materials Conference and Exhibit*, 1998, p. 1927. URL https://ntrs.nasa.gov/search.jsp?R=19980053567.

[15] Panda, B., Mychalowycz, E., and Tarzanin, F. J., "Application of passive dampers to modern helicopters," *Smart Materials and Structures*, Vol. 5, No. 5, 1996, p. 509.

[16] Pritchard, J., "Overview of landing gear dynamics," *Journal of aircraft*, Vol. 38, No. 1, 2001, pp. 130–137. doi:https://doi.org/10.2514/2.2744.

[17] Haskett, T., Breukelman, B., Robinson, J., and Kottelenberg, J., "Tuned-Mass Damper Under Excessive Structural Excitation," *Report of the Motioneering Inc., Guelph, Ontario, Canada*, 2004.

[18] Smith, M. C., "Synthesis of mechanical networks: The inerter," *IEEE Transactions on Automatic Control*, Vol. 47, No. 10, 2002, pp. 1648–1662. doi:10.1109/TAC.2002.803532.

[19] Smith, M. C., and Wang, F.-C., "Performance benefits in passive vehicle suspensions employing inerters," *Vehicle System Dynamics*, Vol. 42, No. 4, 2004, pp. 235–257. doi:https://doi.org/10.1080/00423110412331289871.

[20] Jiang, J. Z., Matamoros-Sanchez, A. Z., Goodall, R. M., and Smith, M. C., "Passive suspensions incorporating inerters for railway vehicles," *Vehicle System Dynamics*, Vol. 50, No. sup1, 2012, pp. 263–276. doi:https://doi.org/10.1080/00423114.2012.665166.

[21] Jiang, J., Matamoros-Sanchez, A., Zolotas, A., Goodall, R., and Smith, M., "Passive suspensions for ride quality improvement of two-axle railway vehicles," *Proceedings of Mechanical Engineering Part F: Journal of Rail and Rapid Transit*, Vol. 229, No. 3, 2015, pp. 315–329. doi:https://doi.org/10.1177/0954409713511592.

[22] Lazar, I., Neild, S., and Wagg, D., "Using an inerter-based device for structural vibration suppression," *Earthquake Engineering & Structural Dynamics*, Vol. 43, No. 8, 2014, pp. 1129–1147.

[23] Zhang, S. Y., Jiang, J. Z., and Neild, S., "Optimal configurations for a linear vibration suppression device in a multi-storey building," *Structural Control and Health Monitoring*, 2016. doi:https://doi.org/10.1002/stc.1887.

[24] Li, Y., Jiang, J. Z., and Neild, S., "Inerter-Based Configurations for Main-Landing-Gear Shimmy Suppression," *Journal of Aircraft*, 2016, pp. 1–10. doi:https://doi.org/10.2514/1.C033964.

[25] Li, Y., Jiang, J. Z., Neild, S. A., and Wang, H., "Optimal Inerter-Based Shock–Strut Configurations for Landing-Gear Touchdown Performance," *Journal of Aircraft*, 2017. doi:https://doi.org/10.2514/1.C034276.

[26] Naghshineh-Pour, A. H., "Structural optimization and design of a strut-braced wing aircraft," Ph.D. thesis, Virginia Tech, 1998. URL `http://hdl.handle.net/10919/36142`.

[27] Grasmeyer III, J. M., "Multidisciplinary design optimization of a strut-braced wing aircraft," Ph.D. thesis, Virginia Tech, 1998. URL `http://hdl.handle.net/10919/36729`.

[28] Zhang, S. Y., Jiang, J. Z., and Neild, S. A., "Passive vibration control: a structure–immittance approach," *Proceedings of the Royal Society of London A: Mathematical, Physical and Engineering Sciences*, Vol. 473, No. 2201, 2017. doi: https://doi.org/10.1098/rspa.2017.0011.

[29] Su, W., "Nonlinear Aeroelastic Analysis of Aircraft with Strut-Braced Highly Flexible Wings," *58th AIAA/ASCE/AHS/ASC Structures, Structural Dynamics, and Materials Conference*, 2017, p. 1351. doi:https://doi.org/10.2514/MSDM17.

[30] Gern, F., Ko, A., Sulaeman, E., Kapania, R., Mason, W., Grossman, B., and Haftka, R., "Passive load alleviation in the design of a strut-braced wing transonic transport aircraft," *8th Symposium on Multidisciplinary Analysis and Optimization*, 2000, p. 4826. doi:https://doi.org/10.2514/MMAO00.

[31] Krenk, S., and Høgsberg, J., "Tuned resonant mass or inerter-based absorbers: unified calibration with quasi-dynamic flexibility and inertia correction," *Proc. R. Soc. A*, Vol. 472, No. 2185, 2016, p. 20150718. doi:https://doi.org/10.1098/rspa.2015.0718.

[32] Moore, G. J., *MSC/NASTRAN design sensitivity and optimization: user's guide, version 68*, MacNeal-Schwendler Corporation, 1994.

[33] Rodden, W. P., and Johnson, E. H., *MSC/NASTRAN aeroelastic analysis: user's guide; Version 68*, MacNeal-Schwendler Corporation, 1994.

[34] Kang, B.-S., Park, G.-J., and Arora, J. S., "A review of optimization of structures subjected to transient loads," *Structural and Multidisciplinary Optimization*, Vol. 31, No. 2, 2006, pp. 81–95. doi:https://doi.org/10.1007/s00158-005-0575-4.

[35] Kamakoti, R., and Shyy, W., "Fluid–structure interaction for aeroelastic applications," *Progress in Aerospace Sciences*, Vol. 40, No. 8, 2004, pp. 535–558. doi:https://doi.org/10.1016/j.paerosci.2005.01.001.

[36] Martí, R., Lozano, J. A., Mendiburu, A., and Hernando, L., "Multi-start methods," *Handbook of Heuristics*, 2016, pp. 1–21. doi:10.1007/978-3-319-07153-4_1-1.

[37] Gonzalez-Buelga, A., Lazar, I. F., Jiang, J. Z., Neild, S. A., and Inman, D. J., "Assessing the effect of nonlinearities on the performance of a tuned inerter damper," *Structural Control and Health Monitoring*, Vol. 24, No. 3, 2017. doi: https://doi.org/10.1002/stc.1879.

[38] Szczyglowski, C. P., Neild, S. A., Titurus, B., Jiang, J. Z., Cooper, J. E., and Coetzee, E., "Passive Gust Loads Alleviation in a Truss-Braced Wing Using Integrated Dampers," *Proceedings of the 17th International Forum on Aeroelasticity and Structural Dynamics, Como, Italy*, 2017.

[39] Hu, X., Shonkwiler, R., and Spruill, M. C., "Random restarts in global optimization," Tech. rep., Georgia Institute of Technology, 2009. URL `http://hdl.handle.net/1853/31310`.

[40] *CS-25 Certification Specifications for Large Aeroplanes*, European Aviation Safety Agency (EASA), 2003.

[41] Wright, J. R., and Cooper, J. E., *Introduction to aircraft aeroelasticity and loads*, Vol. 20, John Wiley & Sons, 2008.

[42] Rajpal, D., and De Breuker, R., "Dynamic Aeroelastic Tailoring of a Strut Braced Wing Including Fatigue Loads," *Proceedings of the 18th International Forum on Aeroelasticity and Structural Dynamics, Savannah, Georgia, USA*, 2019.

[43] "Proposed Special Condition for Installation of Flutter Suppression System: Applicable to Boeing 747-8/-8F," Tech. Rep. Special Condition C-18, European Aviation Safety Agency, May 2011. URL `https://www.easa.europa.eu/sites/default/files/dfu/SC%20C-18%20for%20publication.pdf`, [Online; accessed 12-July-2019].

[44] Konstanzer, P., Enenkl, B., Aubourg, P., and Cranga, P., "Recent advances in Eurocopter's passive and active vibration control," *Annual Forum Proceedings-American Helicopter Society*, Vol. 64, AMERICAN HELICOPTER SOCIETY, INC, 2008, p. 854.

[45] Kerdreux, B., Jouve, J., Marrot, F., Reymond, M., Priems, M., and Dreher, S., "Vibration comfort improvement through active cabin vibration control and its certification on EC130T2," *38th European Rotorcraft Forum*, 2012.